ADVANCED MATERIALS INTERFACES
Open Access
www.advmatinterfaces.de

A Modular, Lego-Like Microfluidic Platform for Multimodal Analysis of Biofilm Formation and Antimicrobial Response

Deema Islayem, Sagar Arya, Nabila Yasmeen, Nicholas Hallfors, Huu Ngoc, Sara Alkhatib, Ioanna Mela, Siddiq Anwar, Vi Khanh Truong, and Anna Maria Pappa**

Biofilms are substantially more resistant compared to free-floating bacteria, highlighting the need for tools capable of real-time analysis under physiologically relevant conditions. A modular microfluidic platform with integrated electrodes is presented for dynamic sampling and monitoring of biofilm formation and response. Its architecture enables natural shear stress variations and allows label-free studies, including optical microscopy and electrical impedance spectroscopy. The platform evaluates biofilm growth, migration, and regrowth and investigates the effect of i) treatment using antibiotics and ii) antimicrobial coatings (i.e., silver nanoparticles) on *Pseudomonas aeruginosa* biofilms, revealing distinct stages of response and persistence in each case. Distinct biofilm behaviors are identified in response to antibiotic treatment as well as after applying an antibacterial coating (i.e., incomplete vs no biofilm eradication). Furthermore, the platform's modularity allows for biofilm migration and regrowth studies via Lego-like connected modules, emphasizing the need for strategies addressing biofilm resilience and regrowth. The system provides a robust, scalable, and biologically relevant alternative to traditional methods for biofilm research. In addition to basic assays, this system is well-suited for clinical environments, where timely and personalized therapeutic decisions are critical for managing biofilm-related infections.

1. Introduction

Biofilms are organized microbial communities that adhere to surfaces such as living tissues and medical devices, enabling microorganisms to survive in extreme conditions due to a protective extracellular matrix.[1] While naturally occurring, biofilms are responsible for 65–80% of chronic infections, such as urinary tract infections and device-associated complications, which often lead to prolonged hospital stays, increased healthcare costs, and long-term patient morbidity.[2] These infections are difficult to treat due to increased resistance to antibiotics and immune responses, highlighting the need for rapid and precise diagnostic tools for personalized treatment.[3,4]

Standard clinical practices largely depend on antimicrobial susceptibility tests conducted on planktonic bacteria, which often underestimate the optimal antibiotic concentrations necessary to eradicate

D. Islayem, S. Arya, N. Yasmeen, N. Hallfors, S. Alkhatib, V. K. Truong, A. M. Pappa
Department of Biomedical Engineering and Biotechnology
Khalifa University
Abu Dhabi 127788, UAE
E-mail: vikhanh.truong@ku.ac.ae; anna.pappa@ku.ac.ae

S. Arya
Czech Advanced Technology and Research Institute (CATRIN)
Palacký University Olomouc
Šlechtitelů 27, Olomouc 77900, Czech Republic

N. Hallfors
Biotechnology Research Center
Technology Innovation Institute (TII)
Masdar City, Abu Dhabi 9639, UAE

The ORCID identification number(s) for the author(s) of this article can be found under https://doi.org/10.1002/admi.202500303

DOI: 10.1002/admi.202500303

H. Ngoc
School of Biomedical Engineering
University of Sydney
Darlington, New South Wales 2006, Australia

I. Mela
Department of Pharmacology
University of Cambridge
Cambridge CB2 1PD, United Kingdom

S. Anwar
Department of Medicine
Sheikh Shakhbout Medical City
Abu Dhabi 11001, UAE

V. K. Truong
Healthcare Engineering Innovation Group
Khalifa University
Abu Dhabi 127788, UAE

A. M. Pappa
Biotechnology Center
Khalifa University
Abu Dhabi 127788, UAE

A. M. Pappa
Center for Catalysis and Separation
Khalifa University
Abu Dhabi 127788, UAE

biofilm-associated infections.[5,6] While traditional diagnostic methods for biofilm detection, such as culture, microscopy, and colorimetric assays (e.g., microtiter plate, tube method, MPEC assay, and Congo red agar plate) remain widely used, they suffer from significant limitations. These include poor detection of polymicrobial biofilms, disruption of biofilm structure during analysis, technical complexity, high cost, and lack of real-time monitoring capabilities.[7,8] Such limitations can result in treatment failures, recurrent infections, and accelerated antimicrobial resistance, highlighting the need for more dynamic and reliable diagnostic tools.

In the human body, biofilms can develop on both biotic surfaces (e.g., host tissues in the oral cavity, circulatory system, or urinary tract) and abiotic surfaces (e.g., medical implants, catheters, or prosthetics) exposed to fluids such as saliva, blood, or urine.[9] However, most traditional biofilm cultivation methods fail to reproduce the dynamic flow conditions found in the human body, often resulting in an inaccurate representation of in vivo biofilm behavior. Advanced flow-based models like Drip-Flow and Rotary Biofilm Reactors have been developed to mimic in vivo environments more accurately.[10,11] These systems require large volumes of media and extensive tubing, limiting their scalability for high-throughput screenings. Engineered microfluidic platforms address these challenges by enabling precise manipulation of small fluid volumes under controlled conditions, making them ideal for real-time biofilm studies and antimicrobial efficacy testing.[12] Furthermore, microfluidics can be seamlessly integrated with detection tools such as optical and electrical sensors to facilitate rapid, non-invasive, and high-throughput monitoring.[13,14]

Microfluidic chips have been widely utilized for biofilm research, focusing on the effects of flow shear stress,[15] antimicrobial treatments,[16] and other environmental parameters[17] on bacterial adhesion and biofilm formation. However, these systems frequently fail to replicate physiologically relevant shear stresses and often rely on labeling techniques for imaging, which can be disruptive to biofilm formation. Moreover, antibiotic efficacy and susceptibility are typically assessed through basic antimicrobial testing, such as live/dead assays, or biofilm eradication evaluation using confocal imaging. Notably, these studies have not addressed critical biofilm behaviors in response to treatment conditions, such as bacterial persistence, biofilm migration, and biofilm regrowth following treatment cessation. These factors are essential for understanding antibiotic efficacy and the mechanism of action. Although a few studies have explored preventive strategies using microfluidic chip models, comprehensive investigations in this area remain limited,[18] despite its promising potential for clinical applications. Only a limited number of platforms integrate simple, multimodal analysis with label-free detection techniques to enable real-time monitoring of biofilm development and antibiotic responses.[19] Table S1 (Supporting Information) illustrates the main differences between the previously published platform and the current work.

In this work, we present a modular bioelectronic microfluidic platform to use in biofilm studies under various physiologically relevant conditions. The platform design, as shown in **Figure 1**, is simple and optimized to avoid clogging or other often encountered bottlenecks in microfluidic-related studies for uninterrupted biofilm growth. The design allows for label-free microscopy as well as electrical impedance spectroscopy, offering unparalleled flexibility for experimental setups that require simultaneous visualization and electrical characterization of biofilms. In addition, we show that it can be easily configured into a multicompartment system using a Lego-inspired approach, enabling the investigation of biofilm regrowth or migration under treatment, which is often overlooked in current platforms and is a critical aspect in antibiotic resistance. Finally, we evaluate the platform using *Pseudomonas aeruginosa* as a biofilm-forming bacterium model, testing three different classes of antibiotics: tetracycline (TE), chloramphenicol (C), and amikacin (AK), and assessing surface treatment with an antibacterial coating of silver nanoparticles.

2. Results and Discussion

2.1. Design and Physiological Relevance of the Modular Bioelectronic Microfluidic Platform

Our platform incorporates four wavy microchannels as shown in Figure 1a, each with a height of 220 µm, specifically engineered to mimic the intricate microscale pockets and dynamic flow conditions characteristic of natural biological environments, such as those found in urinary catheters or in other medical implants.[20,21] The wavy channel geometry creates heterogeneous flow conditions, promoting localized regions of low shear stress. These regions provide a stable microenvironment for biofilm establishment and mimicking actual in vivo conditions more accurately than conventional designs.[22]

To support flexibility and rapid adaptation to different experimental needs, the platform was designed as shown in Figure 1a using a modular architecture inspired by the LEGO-like concept of reconfigurable units. Each chip functions as an independent module that can be combined, rearranged, or replaced depending on the specific biofilm study. This modularity enables scalable study designs and sequential experimentation without the need to redesign the full system. The use of standardized component symmetry allows seamless integration between units, facilitating a plug-and-play approach which reflects the spirit and core principle of LEGO systems, supporting both rapid prototyping and increased-throughput analysis.

Initially, two microfluidic chips with channel heights of 60 and 220 µm were fabricated. However, under static conditions, biofilm thickness was found to reach ≈200 µm, as shown in Figure S1 (Supporting Information). Consequently, the 220 µm channel height was chosen for subsequent experiments, as it is more closely aligned with the observed biofilm behavior. Additionally, in a study by Blanco et al., a microfluidic chip with a thickness of 150 µm was shown to outperform thinner designs (e.g., 50 and 100 µm).[19] The shallower channels resulted in cell filamentation and increased cell death, whereas the 150 µm design supported a uniform, live biofilm covering the entire surface area.[19] These findings further validated our decision to employ the 220 µm thickness, providing a stable environment conducive to biofilm growth.

Studies in literature report a wide range of flow rates, reflecting the diversity of experimental conditions used to model biofilm growth.[19,23,24] In this work, a flow rate of 30 µL min^{-1} was selected to closely mimic physiological conditions, such as urine

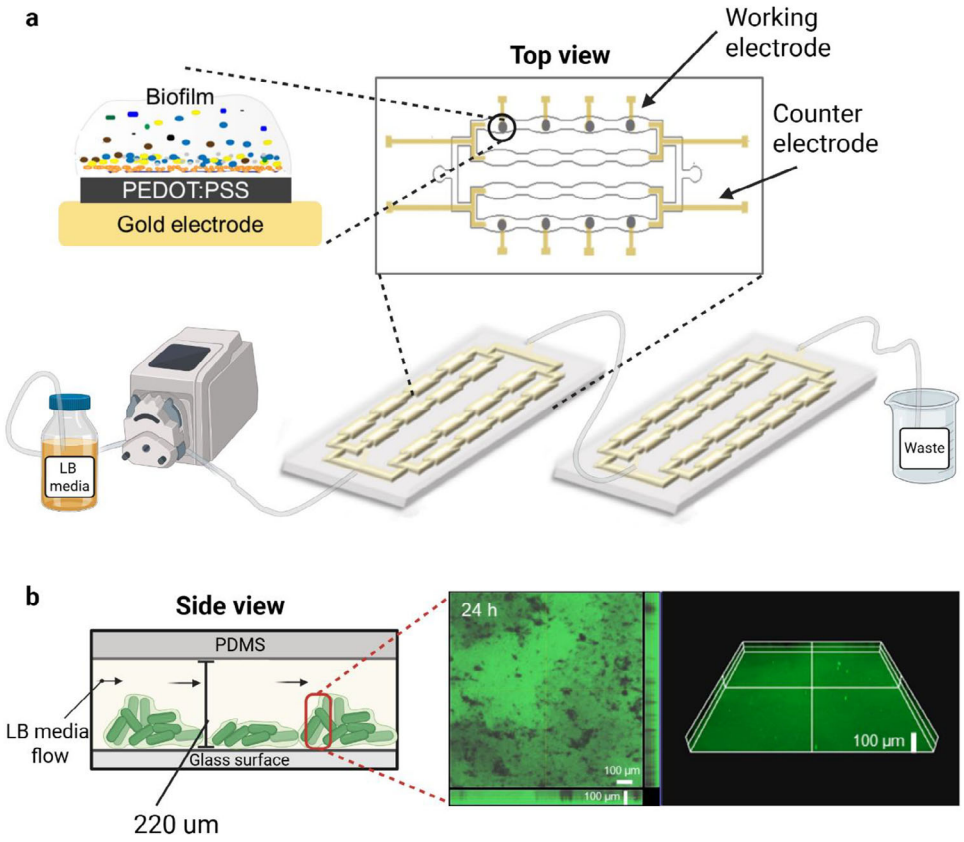

Figure 1. Biofilm on chip design. a) experimental setup of the two microfluidic chips connected ins Lego-like structure to study different conditions of biofilm, including biofilm formation in the first chip and biofilm migration to the second chip. Additionally, the top view of the first chip shows the integrated electrode system that allows the real time, non-disruptive, and label-free detection of biofilm through EIS. b) Schematic representation of biofilm formation as viewed from the side of the chip, and the 100 µm thickness of 24h formed biofilm as imaged via confocal microscope and represented by 3D configuration. The biofilm was stained with FilmTracer SYPRO™ Ruby biofilm matrix stain. The figure is created in https://BioRender.com.

flow in the ureter. This flow rate was calculated based on the ureter's natural diameter and flow dynamics, scaled to match the dimensions of the microfluidic chip.[25] By replicating biologically relevant shear stress and flow dynamics, the platform enables the study of biofilm development and treatment in conditions that closely resemble those in the human body.

We conducted 20 experiments to test the developed design specifications at the selected flow rate. Among these, 18 experiments (93.3%) successfully achieved complete uninterrupted biofilm formation. This high success rate demonstrates the reproducibility and reliability of the design in mimicking biofilm formation dynamics under controlled conditions.

The platform integrates eight working electrodes and four counter electrodes, ensuring experimental accuracy and sensitivity. Each working electrode is gold-coated and functionalized with Poly(3,4-ethylenedioxythiophene) polystyrene sulfonate (PEDOT:PSS). While gold itself is stable and has excellent electrical conductivity, its inherent antibacterial properties could potentially interfere with biofilm formation[26] whereas PEDOT:PSS has shown to support microbial adhesion and biofilm growth while maintaining high electrical conductivity.[27] The polyanionic PSS dopant renders the surface hydrophilic and negatively charged, an environment that encourages initial bacterial adhesion and biofilm formation by retaining a hydrated, ion-rich interface conducive to microbial attachment.[28] Beyond improving compatibility, PEDOT:PSS offers significant advantages for sensing applications: it is a mixed ionic–electronic conductor, allowing it to interact directly with ionic species in the biofilm microenvironment and transduce these fluctuations into sensitive electrical signals. Its inherently low impedance and electrochemical stability further enhance signal quality in impedance-based measurements.[29] Importantly, PEDOT:PSS in its oxidized state also acts as an electron acceptor, facilitating bacterial respiration and promoting biofilm formation.[30]

The side view of the microfluidic chip, shown in Figure 1b, revealed a biofilm thickness of 100 µm as determined by confocal laser scanning microscopy (CLSM). This thickness falls within the range commonly reported in the literature, which varies depending on factors such as flow conditions, nutrient availability, and shear stress.[31] Notably, the thickness observed in this study is higher than that reported in rectangular channel designs, where biofilms of ≈50 µm have been documented.[19] This difference may be attributed to the gentler flow conditions provided by the wavy channel design, which creates a more favorable environment for biofilm development and growth.

2.2. A Modular Microfluidic Platform for Real-Time Monitoring of Biofilm Formation and Dynamics

The modular microfluidic platform developed in this study serves as a comprehensive tool for investigating the dynamics of *P. aeruginosa* biofilm formation, a model organism commonly associated with biofilm-related infections.[32] Unlike conventional microfluidic systems that predominantly focus on endpoint observations, this platform facilitates continuous and detailed monitoring of biofilm progression. This capability provides unprecedented insights into the temporal stages of *P. aeruginosa* biofilm development and behavior under physiologically relevant flow conditions, enhancing our understanding of its pathophysiology in infection settings.

Biofilms were grown within the microfluidic chip over a 48 h period at room temperature under flow conditions, which began 2 h after bacterial injection, as illustrated in **Figure 2a**. Their progression was monitored at regular intervals using optical microscopy as well as high-resolution CLSM. The transparent PDMS construction of the chip also allowed direct visualization of the biofilm with minimal interference. As shown in Figure 2b, biofilm coverage analysis of Figure 2c indicated that biofilm exhibited distinct stages of growth: initial attachment, microcolony formation, maturation, and dispersion. CLSM figures shown in Figure 2d explain the progression of biofilm formation by time, where during the first 2 h, bacterial adhesion occurred predominantly at the corners and walls of the chip, which acted as attachment focal points marking the initial attachment phase. This observation aligns with studies indicating that microfluidic channels with sharp turns exhibit regions of near-zero velocity at the turns, leading to increased cell adhesion in these areas.[33] By 12 h, the biofilm had advanced to the microcolony formation stage. The green fluorescence of the biofilm matrix stain revealed the beginning of 3D matrix formation, indicating the structural organization of the biofilm. Notably, at this stage, increased biofilm accumulation was observed in the outer channels of the device. While this trend was not consistently present across all replicates, it highlights the early-stage heterogeneity of biofilm development, which can occur due to microenvironmental factors influencing initial bacterial attachment. Similar to physiological conditions, where bacterial colonization may initiate in discrete niches before expanding, the observed pattern may result from variations in seeding density or surface conditioning effects. To investigate whether hydrodynamics contributed to this variability, COMSOL simulations were conducted to study velocity and wall shear stress distribution before biofilm formation. Figure S2 (Supporting Information) showed relatively uniform shear stress and velocity across all four channels, suggesting that the observed growth pattern was not flow-driven.

At 24 h, the biofilm fully matured, forming dense, complete 3D extracellular matrix and multilayered growth that completely covered the chip. This stage was selected as the optimal time point for conducting subsequent experiments, including antibiotic treatment studies. By 48 h, the biofilm actively dispersed, with clusters visibly detaching and migrating to other regions of the chip, demonstrating its ability to colonize and disseminate.

To validate the presence and structural integrity of the biofilm, the microfluidic chip was disassembled, and the glass substrate was analysed using SEM. As depicted in Figure 2e, SEM images confirmed dense bacterial growth and well-defined biofilm architecture, providing robust evidence of successful biofilm formation and maturation. The schematic of the SEM image of the biofilm shows that the shear forces generated by the flow impact bacterial adhesion and biofilm development, leading to a heterogeneous distribution of biofilm clusters. Instead of forming uniform layers, the biofilm exhibits localized growth patterns with distinct regions of attachment separated by exposed substrate. The combined imaging techniques demonstrated the platform's ability to capture biofilm dynamics with exceptional clarity and precision.

In addition to the imaging-based characterization, COMSOL simulations were conducted to analyze the impact of progressive biofilm growth on fluid dynamics within the microfluidic chip. As shown in Figure S2 (Supporting Information), at the initial stage (0 h), with no biofilm present, velocity and shear stress distributions were symmetrically distributed across all channels. After 12 h, when biofilm growth was primarily localized to the outer channels, localized narrowing led to a significant decrease in velocity in the outer channels and slightly elevated wall shear stress in those regions, especially near the channel constrictions. This asymmetry disrupted the uniform flow field and created hydrodynamic variability. However, by 24 h, biofilm coverage had expanded uniformly across all channels, effectively restoring symmetry in the flow domain. Consequently, both velocity and shear stress distributions closely resembled the no-biofilm case, despite a reduction in effective channel cross-section. This suggests that once biofilm growth becomes spatially uniform, the system re-stabilizes into a new steady state with consistent hydrodynamic conditions.

While previous studies developed microfluidic systems to study biofilms, they often focus on processes occurring after biofilm formation, such as the effects of specific treatments, rather than investigating the general dynamics of the biofilm formation process itself.[34,35] In contrast, this platform offers a comprehensive and detailed observation of the progression of biofilms by time, representing a significant advancement in understanding biofilm formation dynamics when studied under flow conditions.

2.3. Screening of Antibiotic Treatment and Antibacterial Coating for Therapeutic and Preventive Approaches

We further used this modular microfluidic chamber to study the effect of antibiotics on the biofilm of *P. aeruginosa* as explained in **Figure 3a**. Three selected antibiotics—tetracycline (TE), chloramphenicol (C), and amikacin (AK)—were tested, and their effects were compared to untreated controls. TE and C are broad-spectrum antibiotics effective against both gram-positive and gram-negative bacteria, making them versatile options for treating a wide range of infections.[36,37] Amikacin, on the other hand, belongs to the aminoglycoside class of antibiotics and is widely used for treating infections caused by *P. aeruginosa*.[38] Since the biofilm are more resistant to antibiotics as compared to planktonic bacteria, these antibiotics are used at a concentration that is 4 times above their minimum inhibitory concentration, as shown in Table S2 (Supporting Information). Observations of the

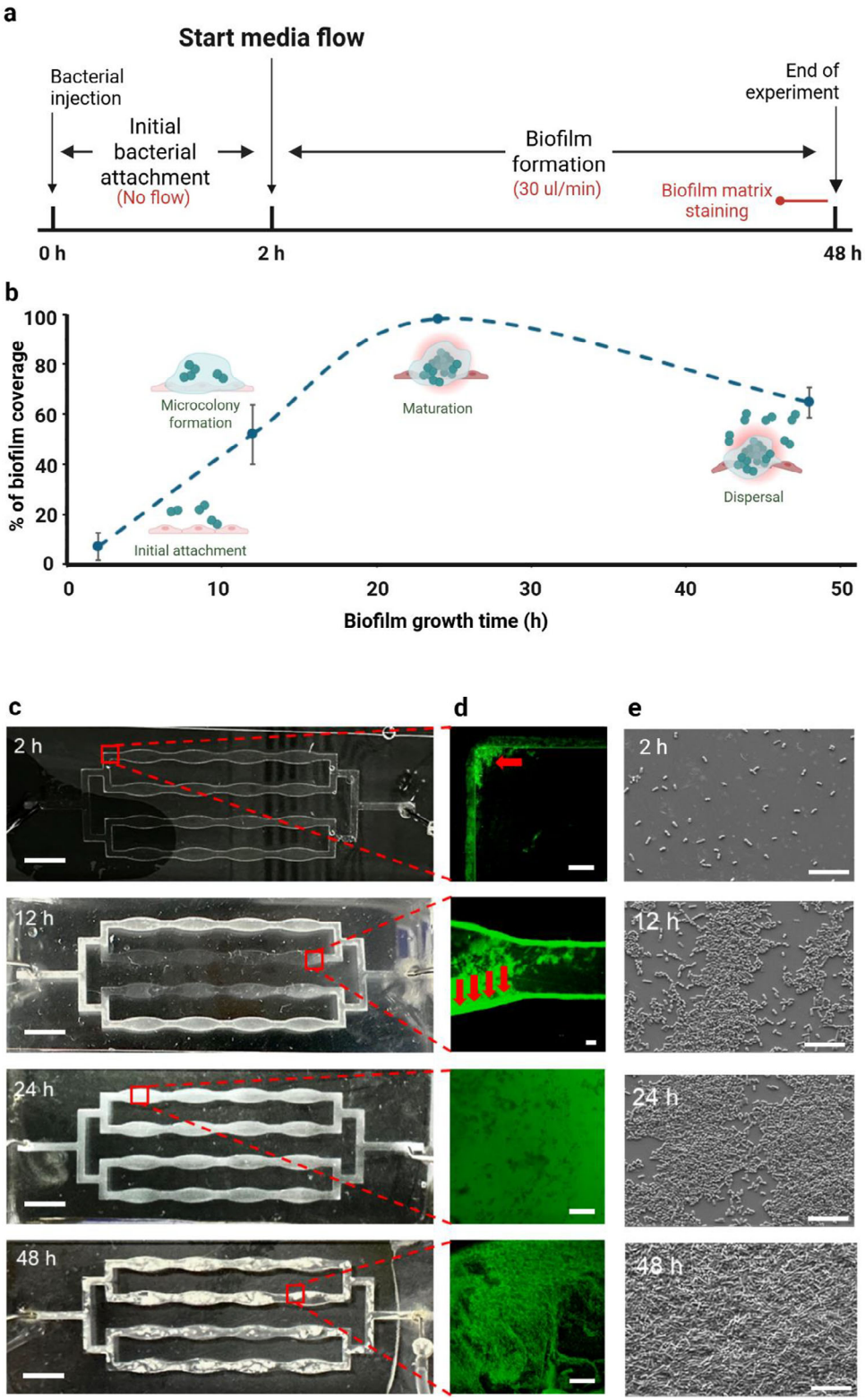

Figure 2. The experimental setup utilizes the modular microfluidic chamber to study biofilm formation under physiologically relevant conditions. a) Timeline for the experimental setup of biofilm formation monitoring. b) % of biofilm coverage inside microfluidic chip as analyzed by ImageJ showing key stages of biofilm growth, from initial bacterial seeding to the maturation and dispersion phases. c) Monitoring biofilm formation over 48 h, visualized both macroscopically (visible to the unaided eye) where the scale bar is 5 mm, and d) microscopically using confocal imaging after staining with FilmTracer SYPRO Ruby biofilm matrix stain to highlight the EPS. The scale bar is 200 µm. e) Scanning electron microscopy for biofilm development inside the microfluidic chip imaged at various time points during the 48 h experiment. The scale bar is 10 µm. The figure is Created in https://BioRender.com.

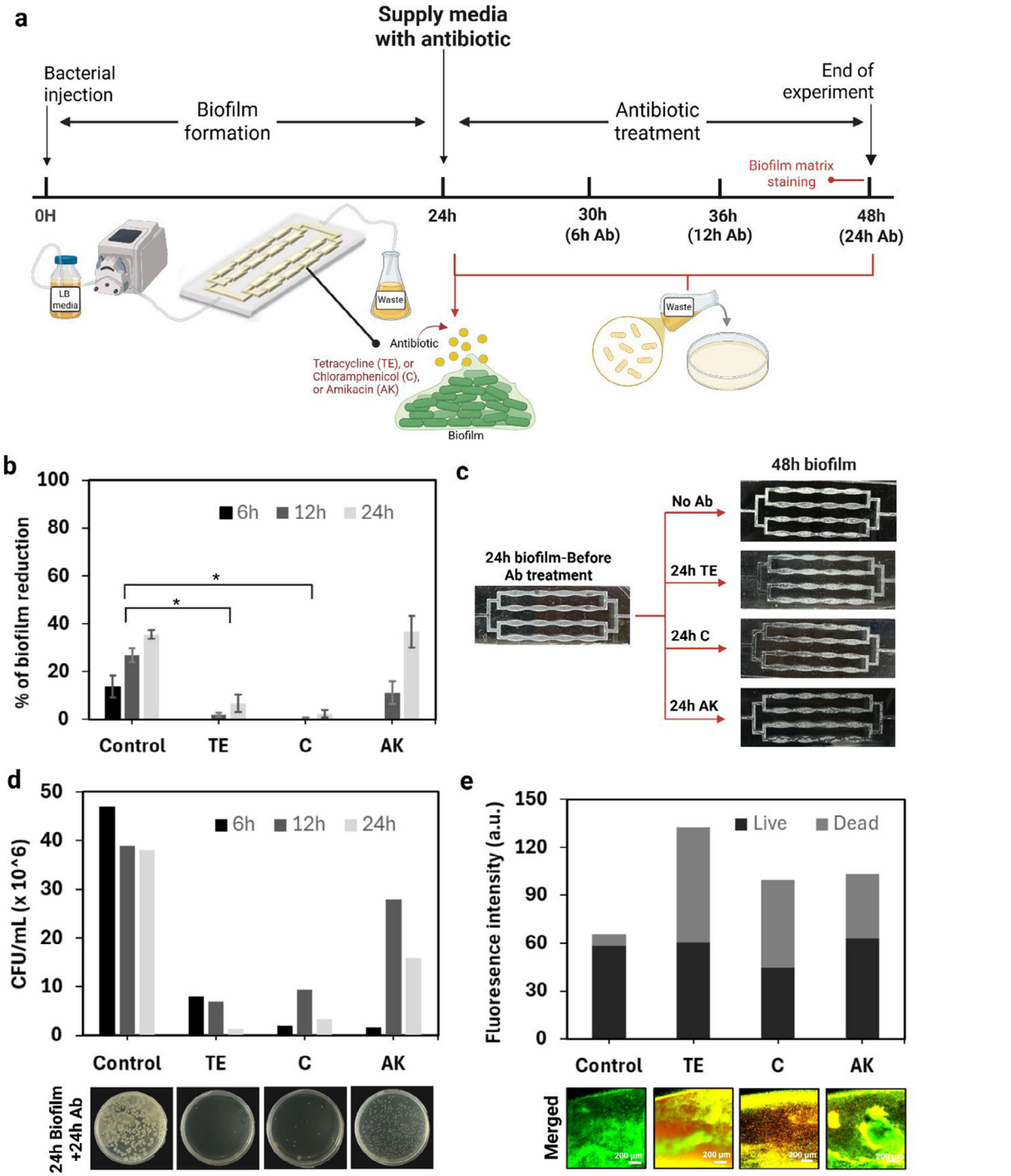

Figure 3. Screening of antibiotic reagents for treating biofilm formation. a) Experimental timeline illustrating the full 48-h protocol. Biofilms were first established for 24 h, followed by antibiotic treatment with TE, C, and AK for 6, 12, or 24 h, with final measurement taken at the 48 h endpoint. b) Quantification of biofilm surface area reduction (in %) after antibiotic treatment, relative to the untreated control. For the control group, 24 h mature biofilm maintained for an additional 6, 12, or 24 h under flow with no antibiotic. Analysis was performed using ImageJ based on the images shown in (c) and (Figure S3, Supporting Information). Biofilms were matured for 24 h before treatment. The experiment was repeated 3 times, and $p < 0.05$ between control and TE, and C treated samples indicating significant difference. c) Representative images of biofilms inside the microfluidic chip: (left) mature biofilm at 24 h, immediately before antibiotic treatment; (top right) untreated control biofilm matured for 24 h and maintained for an additional 24 h without antibiotic treatment (total 48 h); (bottom three) biofilms after 24 h of treatment with TE, C, or AK, following an initial 24 h growth period. Images for 6 h and 12 h treatments are provided in Figure S3 (Supporting Information). d) Colony-forming unit (CFU/mL) counts from the outlet flow, measured before and after antibiotic treatment for 6 h, 12 h, and 24 h. e) Quantification of live and dead biofilm populations based on fluorescence intensity after 24 h of antibiotic treatment, compared to untreated control. Confocal images were captured at 20× magnification. The figure is Created in https://BioRender.com.

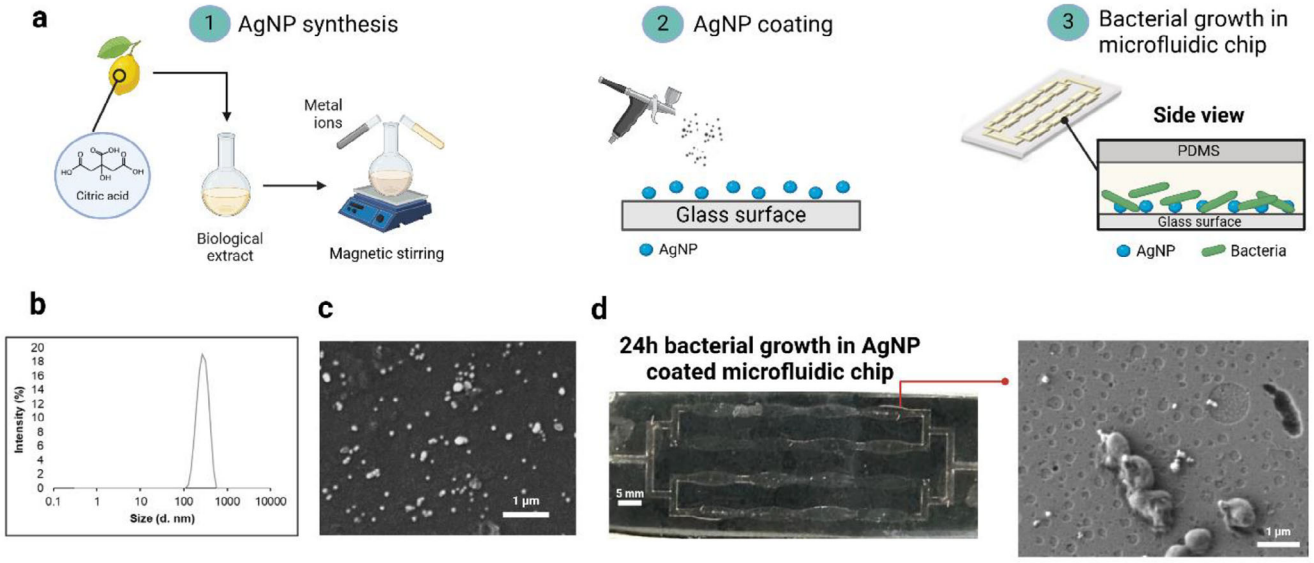

Figure 4. Screening the efficiency of silver nanoparticles coating for preventing biofilm formation. a) Schematics for the experimental setup. b) silver nanoparticles characterization based on size as detected by light dynamic scattering technique, and c) morphology as visualized by SEM. d) visual representation and SEM image of the microfluidic chip after coating its surface with silver nanoparticles and growing the bacteria inside for 24 h. The figure is Created in https://BioRender.com.

microfluidic chip exterior, as illustrated in Figure S3 (Supporting Information) revealed distinct outcomes for each antibiotic.

As shown in Figure 3b,c, untreated biofilms began detaching after 30 h, reducing coverage to ≈35% after 48 h as they entered the dispersion stage. In contrast, TE and C treatments resulted in sustained bacterial reductions, decreasing biofilm coverage by only ≈5% after 24 h. Meanwhile, AK led to a more significant reduction of 37% after 24 h of treatment, compared to the biofilm coverage at 24 h before treatment. These results are consistent with the fact that TE and C inhibit protein synthesis and are bacteriostatic, meaning they halt bacterial growth without actively removing the biofilm, leading to minimal reduction. In contrast, AK is bactericidal, actively killing bacteria and contributing to a more pronounced biofilm reduction, as observed in this study. Direct counting of colony forming units (agar plating) and Live/Dead fluorescence staining were used to further understand the antibiotic behavior.

Interestingly, TE and C treatments showed a significant decrease in the CFU up to 24 h, while AK-treated biofilms exhibited initial CFU decreases only up to 6 h, followed by regrowth after 12 h, indicating limited impact on biofilm persistence (Figure 3d; Figure S4, Supporting Information). Antibiotic-treated biofilms displayed small colony variants (SCVs), a persister cell phenotype triggered by environmental stress like antibiotics, where they enter a dormant state characterized by slow growth and reduced metabolic activity. SCVs were also detected in untreated biofilms due to nutrient depletion and waste accumulation but were more prevalent in treated samples.[39]

In Live/dead fluorescence staining, live bacteria fluoresce green due to SYTO 9 dye uptake, while dead or membrane-damaged cells fluoresce red due to propidium iodide penetration. This staining assay confirmed higher non-viable cell levels for antibiotic treated samples compared to controls (Figure 3c; Figure S5, Supporting Information). Specifically, TE and C treatments produced pronounced red fluorescence, indicating a higher proportion of membrane-compromised of dead bacterial cells, which reflects stronger effects of these treatments. However, residual biofilm structures still persisted, driven by dormancy mechanisms such as the stringent response, which slows metabolism and promotes persister cell formation.[40,41] These findings highlight the biofilm's ability to survive the antimicrobial treatment and pose a significant challenge in clinical applications as a potential reservoir for future infection or recolonization.

The modular microfluidic chamber was used to demonstrate its versatility in evaluating surface coating strategies to prevent biofilm formation. To explore this capability, the chamber's surfaces were precoated with green-synthesized silver nanoparticles (AgNPs), prepared using lemon juice as a reducing agent, as shown in **Figure** 4a. This environmentally friendly synthesis method avoids toxic chemicals typically used in nanoparticle fabrication, offering a safer and sustainable alternative.[42]

The AgNPs were characterized for their physicochemical properties. A peak absorbance at ≈415 nm was oserved after 2 h of incubation, indicating successful stabilization. Zeta potential measurements indicated a negative charge of –20 mV, confirming stability through electrostatic repulsion (Figure S6, Supporting Information). Dynamic light scattering techniques showed that the AgNPs are with an average size of 267 nm (Figure 4b), and SEM imaging revealed a spherical structure in nanometre size (Figure 4c).

The AgNP-coated microfluidic chip effectively inhibited biofilm formation during a 24 h flow of LB media. SEM imaging confirmed the absence of mature biofilms, with only isolated bacterial cells observed, most of which were structurally damaged or non-viable (Figure 4d). These findings provide direct evidence

of the efficacy of AgNP coatings in preventing biofilm establishment under physiologically relevant flow conditions.

This study highlights a multimodal modular microfluidic platform for testing preventive strategies against biofilm formation, particularly the use of different coating strategies. Unlike previous study focusing on the therapeutic effects of AgNPs on preformed biofilms,[43] here we show the pre-emptive potential of AgNPs in biofilm growth inhibition. This microfluidic approach enables real-time evaluation of various nanoparticle coatings and the fate of biofilms, expanding the possibilities for engineering antimicrobial surfaces suited to dynamic environments such as those encountered in medical devices.

2.4. Multicompartment Tool for Optical and Electrical Assessment of Biofilm Migration and Regrowth After Antibiotic Treatment

To investigate biofilm migration (or recolonization) potential, a multicompartment modular microfluidic chamber was employed (**Figure 5a**). Understanding biofilm migration is critical, as it contributes to the recurrence and spread of infections, particularly in medical settings. This setup evaluated the biofilm's ability to migrate, recolonize new surfaces, and regrow after antibiotic removal, simulating clinically relevant scenarios.

In this study, once the biofilm of ≈90% coverage was formed in the first chip, a second chip was connected through the outlet; and the system was exposed to the continuous flow of antibiotic-containing media for 24 h. The second chip was then monitored to detect any possible migration of the antibiotic-treated biofilm from the first chip. As shown in Figure 5b and Figure S7 (Supporting Information), mature biofilm formation was observed on the non-treated (control) samples, with ≈70% coverage in the second chip, as expected. TE and C treated samples showed minimal biofilm transfer to the second chip, while AK treatment showed higher migration potential, consistent with the observed growth using agar plates of Figure 3d. Following the cessation of antibiotic treatment, fresh medium without antibiotic supplements was then introduced to evaluate any potential for biofilm regrowth in the second chip. Indeed, significant biofilm regrowth was observed across all treated samples, highlighting the resilience and adaptability of *P. aeruginosa* biofilms. This rapid regrowth underscores the limitations of existing therapeutic strategies in fully eradicating biofilm and emphasizes the role of dormant persister cells. These cells are protected during antibiotic exposure by survival mechanisms like the stringent response, reactivated after treatment ceased, leading to recolonization and renewed biofilm activity.[44]

Clinically, these findings highlight the risk of incomplete biofilm removal, as migrating fragments or planktonic bacteria can spread to new sites, potentially exacerbating recurrent infections.[45] While antibiotics were found to pause biofilm migration in the second chip initially, the observed regrowth after treatment highlights the need for enhanced treatment strategies targeting both active and dormant populations, as well as optimized antibiotic types, dosages, and durations.

From a clinical perspective, the capability to accurately and rapidly detect real-time changes in biofilm formation, disruption, and regrowth is critical. To achieve this, electrodes can be easily integrated into the first chip, enabling real-time electrochemical impedance spectroscopy (EIS) measurements. Unlike optical methods that require invasive imaging, EIS provides continuous, non-disruptive monitoring with exceptional sensitivity. Initially, we confirmed that the electrical interrogation itself does not influence biofilm development by altering the oxidation state or surface properties of PEDOT:PSS. Therefore, a control study was conducted where biofilm growth was compared on PEDOT:PSS-coated electrodes that underwent impedance measurements versus electrodes left pristine without electrical stimulation. As shown in Figure S8 (Supporting Information), SEM imaging showed no observable differences in biofilm coverage, morphology, or density between the two groups, confirming that the applied measurements did not disrupt surface conditions or biofilm behaviour. EIS measurements were recorded using a frequency range from 0.01 Hz to 100 kHz at open circuit potential (OCP) (bode plot in Figure S9, Supporting Information). Nyquist plots (Figure 5c) revealed changes in charge transfer resistance (Rct) (Figure 5d), offering deeper insights into biofilm behaviour during growth, treatment, and regrowth phases. The visual appearance of the biofilm inside the bioelectronic chip is shown in Figure S10 (Supporting Information).

A notable change in impedance was observed in the Nyquist plot after biofilm formation which is most probably because of high biofilm coverage on PEDOT:PSS coated gold electrodes, which also resulted in a high Rct value. Laterally, biofilm was exposed to TE treatment for the next 24 hr resulting in an increase in impedance in Nyquist plot. This shift toward higher Rct likely occurred because of high accumulation of dead bacteria as debris, most probably under treatment the bacterial cells in the biofilm became dormant and leaving debris strongly adhered to the electrodes that hindered the charge transport. After that, the microfluidic platform was washed thoroughly with sterile filtered 1X PBS buffer (pH 7) to ensure complete removal of debris and antibiotic solvent. Then, fresh media was added to the system under flow conditions to observe whether bacteria in biofilm were killed under TE treatment or went under dormant stage. Surprisingly regrowth of biofilm was observed within 24 hrs. The obtained Rct values for new biofilm was approximately similar to initial biofilm growth before treatment. This indicates that TE treatment was not able to entirely kill bacteria in biofilm and eradicate it where the dormant bacteria were reactivated and resulted in fresh biofilm formation within 24 hr.

To complement the main EIS analysis, we also evaluated amikacin (AK), a representative bactericidal antibiotic. As shown in Figure S11 (Supporting Information), the response followed a similar trend to TE, showing increased Rct after treatment. However, AK resulted in lower overall Rct values (Table S3, Supporting Information), consistent with its observed increased biofilm reduction efficacy (see Figure 3b,c).

This study highlights the efficiency of combining modular microfluidics with advanced electrical measurements to study biofilm dynamics. By integrating PEDOT:PSS-coated electrodes for enhancing surface area and sensitivity, the platform was able to monitor of biofilm formation, treatment efficacy, and post-treatment regrowth under flow conditions. Although we can get a good estimation of biofilm formation and treatment on our PEDOT:PSS incorporated electrodes using EIS studies, further understanding of the electrochemical footprint of biofilms based on

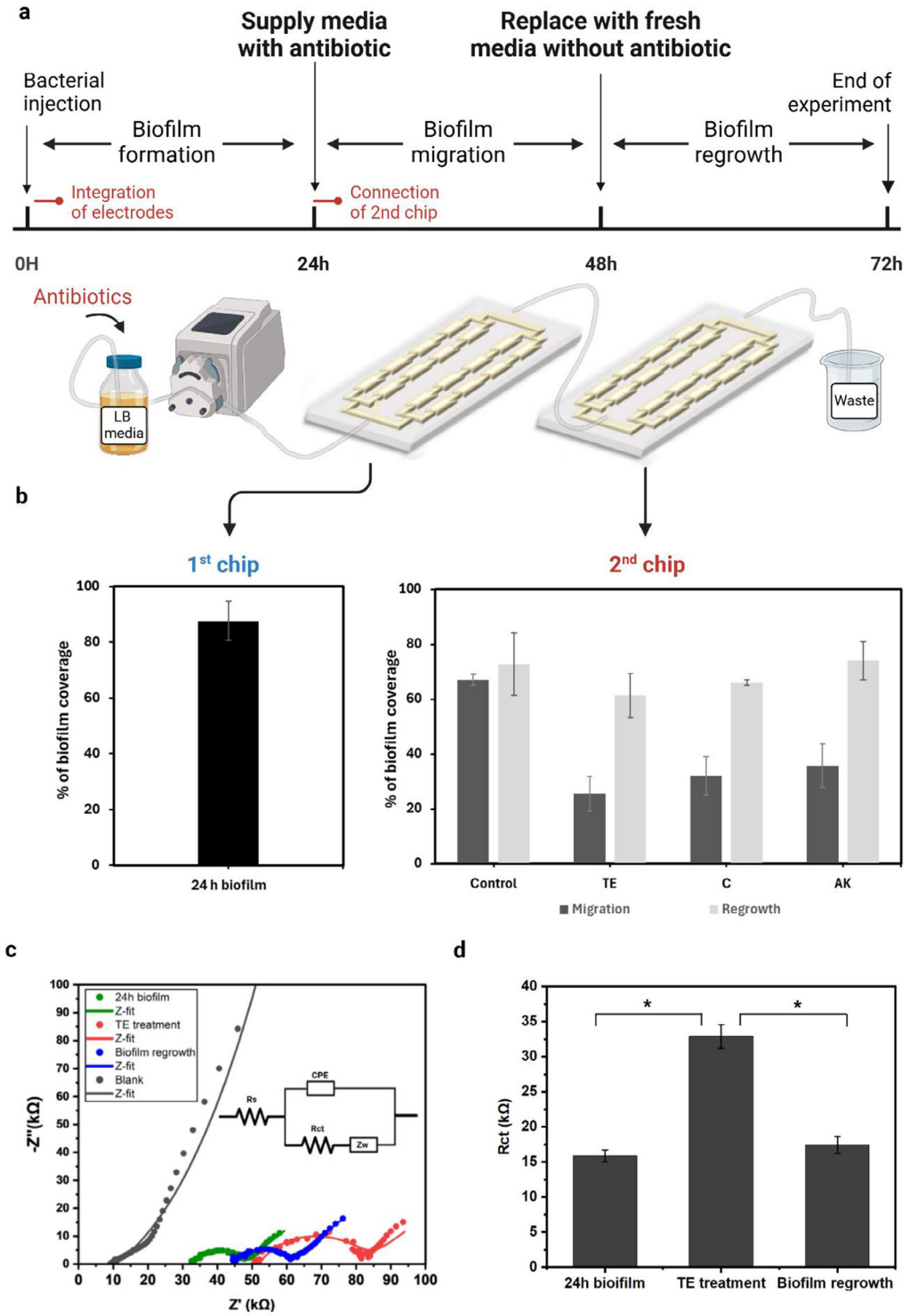

Figure 5. Assessing biofilm migration and regrowth to another site after the antibiotic treatment, and electrical impedance spectroscopy measurement for the different conditions: biofilm growth, biofilm treatment, and biofilm regrowth. a) Timeline and graphical representation of the experimental setup where two microfluidic chips are connected in LEGO-like setup. b) Quantification of % biofilm coverage in the first and second microfluidic chips. Biofilm in the first chip was allowed to mature for 24h. After connecting the second chip, antibiotic-containing media was supplied for 24h (24–48h). Biofilm detected in the second chip at 48h is attributed to migration under flow. Antibiotic-free media was then introduced from 48–72h, and additional biofilm formation in the second chip at 72h is attributed to regrowth. Data represents average values from 3 independent experiments. c) real time EIS monitoring of biofilm formation, removal by TE treatment, and regrowth after TE cessation. Additionally, the circuit used to fit the data is shown, along with d) Rct analysis from the zfit data of the Nyquist plot. Measurements were taken 3 times, and $p < 0.05$ between 24h biofilm and treated biofilm, and between treated biofilm and regrew biofilm after antibiotic cessation, indicating a significant difference. The figure was Created in https://BioRender.com.

the bacteria type is needed. This could open new directions on the mechanistic understanding of biofilm behaviour and establish electronic methods as a standalone tool for assessing biofilms in clinically relevant settings.

3. Conclusion

We have developed a modular microfluidic chamber for studying biofilm behavior and evaluating new antibiofilm strategies. Our platform integrates microfluidics and bioelectronics, offering real-time, continuous, and non-disruptive monitoring of biofilm dynamics. Its modular design provides notable flexibility, enabling the study of key biofilm processes, including formation, migration, persistence, and regrowth, under flow conditions. By mimicking clinically relevant scenarios, we have revealed critical insights into biofilm resilience, including the regrowth and recolonization that occur after antibiotic treatment cessation. This platform can be readily applied in fundamental biofilm research, antimicrobial screening, and early-stage drug discovery. Its portability, enabled by the use of low-cost materials and a simple, scalable, compact setup, further supports its practical potential outside conventional laboratory settings. For broader translation into clinical use, further improvements such as automation and integration with user-friendly data acquisition tools will be needed.

4. Experimental Section

Bacterial Growth Condition: *Pseudomonas aeruginosa* (ATCC 15692) was revived from a glycerol stock by streaking onto an LB agar plate, followed by incubation at 37 °C for 24 h. Single colonies were then picked up and inoculated into LB broth, which was incubated in a shaker incubator at 120 rpm and 37 °C for 24 h. After incubation, the optical density (OD) of the bacterial culture representing its growth was measured at a wavelength of 600 nm using a plate reader. The culture was subsequently diluted with fresh LB broth to an OD of 0.2, representing the exponential growth phase, making it ready for further experiments.

Microfluidic Chip Design and Fabrication: The microfluidic chip was designed using AutoCAD software (Autodesk, USA) and consisted of four channels with four cisterns each, along with an inlet and outlet. The design of the chip is inspired by the study of Bourguignon et al.[46] with a few modifications where the chip dimensions are shown in Figure S12 and Table S4 (Supporting Information). The overall 3D dimensions of the chip were 60 mm × 16 mm × 220 µm. The design incorporated four main channels to monitor biofilm growth at various locations within the chip, ensuring uniform biofilm formation across all locations.

To fabricate the mold for the microfluidic chip, SU-8 100 photoresist (MicroChem, Germany) was spin-coated onto a silicon wafer substrate. Initially, the photoresist was spread at 500 rpm with an acceleration of 100 rpm/sec for 10 s, followed by a final spin at 3000 rpm with an acceleration of 300 rpm/sec for 30 s. The silicon wafer was then soft baked for 5 min at 65 °C, followed by 20 min at 95 °C to evaporate the solvent, densify the film, and prepare it for crosslinking.

Next, the chip design pattern was transferred onto the photoresist-coated wafer using laser lithography. Then, a post-exposure bake was performed, first for 1 min at 65 °C, then for 10 min at 95 °C, to selectively crosslink the exposed portions of the SU-8 film corresponding to the design. The wafer was then developed by immersing it in SU-8 developer with gentle stirring for ≈10 min, rinsed with isopropanol for 10 s, and blow-dried with nitrogen to remove residual isopropanol. A hard bake was conducted at 95 °C for 2 min to cure the film and evaporate any remaining liquid, resulting in the pattern adhering firmly to the substrate.

Following this, Deep Reactive Ion Etching (DRIE) was performed to achieve the desired feature height, with the SU-8 serving as an etch mask. Bosch process plasma etching was conducted with 400 cycles to achieve a final depth of 220 µm. Finally, the master mold was treated to become hydrophobic to facilitate the release of PDMS in chip production.

To produce the microfluidic devices, poly(dimethyl siloxane) (PDMS) was prepared by mixing PDMS prepolymer and a curing agent (Sylgard®184, Dow Corning) at a 10:1 ratio. This mixture was poured onto the fabricated mold and baked at 100 °C for 20 min to solidify the PDMS. The PDMS was then carefully cut around the mold design and peeled off, retaining the chip pattern. Inlet and outlet holes were punched using a 0.5 mm diameter puncher.

The PDMS chip and a glass slide were both oxygen plasma treated at 1000 watts for 20 s. Immediately after plasma treatment, the treated surfaces of the PDMS and the glass slide were bonded together, and by baking at 105 °C for 10 min to ensure strong adhesion.

Experimental Setup: The inlet and outlet of the PDMS chip were connected to silicon tubing through 22G needles (0.7 mm diameter). These needles fit securely into the inlet and outlet ports, which were punched with a 0.5 mm ID punch. The inlet tubing was connected to a syringe pump, while the outlet tubing was directed into a 50 mL Falcon tube, which served as a waste container (Figure S13a, Supporting Information).

The microfluidic chip was first sterilized by flushing it with 70% ethanol for 20 min. During this sterilization step, the flow rate was kept low, at no more than 30 µL min^{-1}, then gradually increased to 100 µL min^{-1} to remove any air bubbles that may have formed inside the chip. After sterilization, sterile LB media flowed through the chip for 20 min to flush out any residual ethanol.

Once sterilized, the tubing was disconnected from the PDMS chip, and a bacterial culture, diluted to an OD of 0.1, was injected into the chip using a syringe until the entire chip was filled. To prevent evaporation of the bacterial culture within the chip, drops of sterile LB media were placed at both the inlet and outlet. The bacterial culture was left in the chip for 2 to 3 h without any flow to promote initial bacterial attachment.

After this incubation period, the tubing was reconnected to the chip and attached to the syringe pump, allowing LB sterile media to flow through the system at a constant flow rate of 30 µL/min for 48 h. The whole experiment was carried out at room temperature.

Computational Fluid Dynamics Characterization: Computational fluid dynamics simulations were performed using COMSOL Multiphysics (v6.2) to analyse velocity and shear stress distribution within the wavy-channel microfluidic chip during various stages of biofilm development. A 2D geometry based on the actual CAD design of the device was imported. The fluid domain was modelled as water, with standard properties, and a flow rate of 30 µL min^{-1} was applied at the inlet to match experimental conditions. To simulate biofilm development, the biofilm-covered regions were modelled as porous material using the Brinkman equation with a porosity of 0.7 and a permeability of 1×10^{-12} m^2. The rest of the chip was simulated using the standard laminar flow module. A no-slip condition was applied at all channel walls, and pressure was set to zero at the outlet. An extra fine mesh was used to discretize the geometry, ensuring convergence and high resolution for velocity and shear stress distribution profiles across the device. Shear stress and velocity distributions were computed for three representative time points: 0 h (no biofilm), 12 h (partial biofilm growth), and 24 h (uniform biofilm coverage).

Antibiotic Treatment of Biofilm: Three antibiotics, tetracycline (TE), chloramphenicol (C), and amikacin (AK) were used to evaluate their effectiveness against the biofilm. Before use in the microfluidic chip, each antibiotic was tested on an agar plate. Briefly, Pseudomonas aeruginosa was streaked onto agar plates, and antibiotic disks containing the respective antibiotics were placed on the surface. The plates were incubated at 37 °C for 24 h, after which the bacterial inhibition around each antibiotic disk was observed, indicated by the formation of a clear inhibitory zone. This confirmed the antibiotics' ability to inhibit bacterial growth.

Once confirmed, the antibiotics were introduced into the microfluidic chip. When the biofilm had formed inside the chip after 24 h, the flow of LB media was stopped and replaced with fresh LB media supplemented with the antibiotic above its minimum inhibitory concentration (30 µg mL^{-1}). The antibiotic-supplemented media then flowed through the chip for 24 h.

Colony Forming Unit From Effluent: Another method used to evaluate the effect of antibiotics on biofilm is by measuring the colony-forming units (CFU). Briefly, 30 µL of the media collected from the outlet of the chip was plated onto LB agar plates. The plates were incubated at 37 °C for 24 h, after which the number of bacterial colonies was counted. This experiment was conducted both before antibiotic treatment and at various time points after treatment, i.e, 6, 12, and 24 h.

Confocal Laser Microscope for Live/Dead Assay and Biofilm Staining: The biofilm is stained using two dyes: FilmTracer SYPRO Ruby Biofilm Matrix Stain (Invitrogen), and SYTO 9 dye with propidium iodide from the LIVE/DEAD BacLight Bacterial Viability Kit (Invitrogen). For both stains, after biofilm formation inside the microfluidic chip, the flow of LB media is stopped and replaced with PBS at a flow rate of 30 µL min^{-1} for 10 min to wash the biofilm. The PBS is then replaced with either the biofilm matrix stain or the live/dead stain. The stain is flowed through the chip for 5 min, after which the flow is halted, and the chip is then incubated in the dark for 15 min with the live/dead stain and 30 min with the biofilm matrix stain.

Following incubation, the chip is washed with PBS for 10 min at a flow rate of 30 µL min^{-1} to remove excess stain, and the sample is prepared for imaging using a confocal laser microscope (Olympus).

Scanning Electron Microscopy: The morphology of biofilm is examined using Scanning electron microscopy (SEM, JEOL JSM-7610F). Each microfluidic chip is used for a single time point of biofilm formation, with SEM analysis conducted after 12, 24, and 48 h. At each of these time points, the flow of LB media is stopped and replaced with PBS for 10 min at a flow rate of 30 µL min^{-1} to wash the biofilm and remove any residual contaminants or media. Following the PBS wash, 2% glutaraldehyde is introduced to fix the biofilm. The glutaraldehyde flows through the chip for 10 min, after which the flow is stopped, and the biofilm is incubated in glutaraldehyde for 1 h.

After fixation, the biofilm undergoes a dehydration process using a series of ethanol solutions with increasing concentrations: 60%, 70%, 80%, 90%, and finally 100% ethanol. Each concentration is flowed through the chip for 10 min at 30 µL/min. Once dehydration is complete, the PDMS chip is left in the air to dry.

To prepare the sample for SEM, the PDMS is peeled off the glass slide with care to avoid disrupting the biofilm structure. The glass slide is then cut using a glass cutter to produce a sample size suitable for SEM analysis.

Assessment of Biofilm Migration and Regrowth Using the Lego-Like Multicompartment Setup: To evaluate biofilm migration and regrowth after antibiotic treatment, a two-chip modular microfluidic system was assembled (Figure S13b, Supporting Information). The first chip was inoculated with *P. aeruginosa* and incubated under a continuous flow of LB media for 24 h to allow for mature biofilm formation. At the 24 h time point, a second identical chip was connected, and the system was supplied with LB media containing one of the three antibiotics TE, C, and AK for an additional 24 h (24–48 h). Biofilm presence in the second chip at 48 h was considered indicative of biofilm migration, defined as the detachment and downstream recolonization of viable bacterial clusters or cells under flow. After 48 h, the inlet was flushed and replaced with fresh, antibiotic-free LB media. The system was maintained under continuous flow for an additional 24 h (48–72 h) to assess biofilm regrowth. Coverage in the second chip at 72 h was attributed to the expansion of migrated or surviving bacteria in the absence of antibiotic pressure. Image analyses were used to quantify biofilm coverage at both time points. No interruption in flow was applied between timepoints; instead, time-resolved imaging was used to distinguish migration from regrowth.

Silver Nanoparticle Synthesis and Characterization: Silver nanoparticles (AgNPs) were synthesized by a green method using lemon juice as the reducing agent. Briefly, 50 mM of 50 mL AgNPs were prepared by dissolving 0.4 g silver nitrate (99.99%, Sigma) in 47.5 mL distilled water. The solution was then heated on a magnetic stirrer hot plate set to 75 °C. While stirring, 2.5 mL of lemon juice was added dropwise. The solution was maintained on the hot plate for 2 h, during which 30 µL aliquots were collected every 30 min to characterize the nanoparticles by measuring their absorbance across the full wavelength spectrum. This analysis was used to determine the optimal incubation time. The solution's color change was monitored throughout the process, eventually turning brown, indicating the formation of AgNPs. After incubation, a 30 µL aliquot of the solution was placed on a coverslip, dried on a hot plate, and fixed for SEM imaging. Additionally, 1 mL of the solution was analyzed using a Zetasizer to determine its zeta potential and hydrodynamic size. The prepared AgNP solution was then centrifuged at maximum speed for 15 min. The supernatant was discarded, and the pellet was resuspended in distilled water to obtain the final AgNP solution.

Microfluidic Chip Coating with Silver Nanoparticles: The glass slide of the microfluidic chip was coated with AgNPs as follows. After fabricating the chip, a lightly boiled piranha solution (3:1 v/v of 98% H_2SO_4 and 30% H_2O_2) was flowed through the chip for 20 min to clean the surface. The chip was then thoroughly washed with ultrapure water. Next, the glass slide surface was functionalized with amino groups by flowing a 1% ethanol solution of APTES (3-aminopropyltriethoxysilane) through the chip for 30 min at room temperature. Afterward, the chip was washed with ethanol and cured in a vacuum oven at 100 °C for at least 2 h to ensure full condensation of the APTES molecules onto the glass surface. Following surface functionalization, the AgNP solution flowed into the chip and was allowed to remain for 24 h to enable proper deposition. After incubation, the chip was rinsed with ethanol to remove any unbound particles from the glass surface, dried in vacuum oven at 100 C for 2 h, then bacteria were injected for biofilm experiments as previously described.[47]

Electrical Impedance Spectroscopy Measurement: PEDOT: PSS solution is prepared by mixing with ethylene glycol (5% w/v), DBSA (0.5% w/v), and GOPs (1% w/v). After adding each of the above solutions in order, PEDOT: PSS is sonicated for 10 min at 20 °C. The final solution at the end is filtered with 0.45 um filter.

The developed microfluidic chip is integrated with a gold electrode for electrical impedance spectroscopy measurement as shown in Figure S13c (Supporting Information). The working electrodes were designed to have a circular shape placed in the channels at different locations, so it provides more areas for monitoring biofilm formation to account for errors in the experiment and to confirm the sensitivity of the results. The counter electrode surface area was around three times more than the working electrode, and it is placed at the beginning and the end of the microfluidic chip having a rectangular like shape. The gold electrodes were coated on a glass slide using PVDF machine. Firstly, the glass slide is plasma cleaned to remove any particles attached to it, then titanium layer of 20 nm thickness is coated on the glass slide, followed by a gold coating of 100 nm thickness. The use of the titanium layer was to support gold adhesion and attach to the glass slide without peeling. After that, the working electrodes were spray coated with PEDOT:PSS. Then, the glass slide coated with gold and PEDOT:PSS were sticked to PDMS microfluidic chip after oxygen plasma treatment to get the final microfluidic bioelectronic chip. The device used to record EIS values was PalmSens4 impedance analyzer. This equipment allowed measuring the impedance along a range of frequencies with an oscilloscope level of 0.01 V. The impedance was measured in the module and phase format and plotted in Bode and Nyquist diagrams. Once the microfluidic device was connected, impedance measurements were recorded on 3 working electrodes at different time points of biofilm formation and removal process. Impedance measurements were taken also with 100 mM $K_3[Fe(CN)_6]$ electrolyte solution which is added after mature biofilm formation.

Image and EIS Analysis: Images of the microfluidic chip showing the biofilm formation were analyzed for biofilm surface coverage and reduction percentage using ImageJ. Error bars represent the values from three replicates. The EIS data were analyzed and fitted into a circuit model using EC-Lab, with error bars calculated from three replicates. One way Anova was used to measure statistical significance.

Supporting Information

Supporting Information is available from the Wiley Online Library or from the author.

Acknowledgements

The authors acknowledge Core Technology Platforms (CTPs) of New York University Abu Dhabi (NYUAD) and Dr. Qiang Zhang for assisting with microfabrication. We also acknowledge Khalifa University and the Center for Catalysis and Separations (CeCaS) support (grant no. RC2-2018-024) and the financial support from FSU-2022-009 grant.

Conflict of Interest

The authors declare no conflict of interest.

Data Availability Statement

The data that support the findings of this study are available from the corresponding author upon reasonable request.

Keywords

antibiotic, biofilm, EIS, microfluidic

Received: April 6, 2025
Revised: June 2, 2025
Published online:

[1] H.-C. Flemming, J. Wingender, *Nat. Rev. Microbiol.* **2010**, *8*, 623.
[2] M. Assefa, A. Amare, *Infect Drug Resist* **2022**, *15*, 5061.
[3] P. D. Martino, *AIMS Microbiol* **2018**, *4*, 274.
[4] P. Bowler, C. Murphy, R. Wolcott, *Antimicrob Resist Infect Control* **2020**, *9*, 162.
[5] X. Kang, X. Yang, Y. He, C. Guo, Y. Li, H. Ji, Y. Qin, L. Wu, *Mater Today Bio* **2023**, *23*, 100827.
[6] V. Waters, F. Ratjen, *Cochrane Database of Systematic Reviews* **2017**, https://doi.org/10.1002/14651858.CD009528.pub4.
[7] European Committee for Antimicrobial Susceptibility Testing (EUCAST) of the European Society of Clinical Microbiology and Infectious Diseases (ESCMID), https://doi.org/10.1046/j.1469-0691.2000.00149.x.
[8] J. J. Harrison, C. A. Stremick, R. J. Turner, N. D. Allan, M. E. Olson, H. Ceri, *Nat. Protoc.* **2010**, *5*, 1236.
[9] L. Yuan, H. Straub, L. Shishaeva, Q. Ren, *Annu. Rev. Anal. Chem.* **2023**, *16*, 139.
[10] D. M. Goeres, M. A. Hamilton, N. A. Beck, K. Buckingham-Meyer, J. D. Hilyard, L. R. Loetterle, L. A. Lorenz, D. K. Walker, P. S. Stewart, *Nat. Protoc.* **2009**, *4*, 783.
[11] J. R. Lawrence, G. D. W. Swerhone, T. R. Neu, *J Microbiol Methods* **2000**, *42*, 215.
[12] G. Velve-Casquillas, M. Le Berre, M. Piel, P. T. Tran, *Nano Today* **2010**, *5*, 28.
[13] A.-M. Pappa, V. F. Curto, M. Braendlein, X. Strakosas, M. J. Donahue, M. Fiocchi, G. G. Malliaras, R. M. Owens, *Adv. Healthcare Mater.* **2016**, *5*, 2295.
[14] V. F. Curto, B. Marchiori, A. Hama, A.-M. Pappa, M. P. Ferro, M. Braendlein, J. Rivnay, M. Fiocchi, G. G. Malliaras, M. Ramuz, R. M. Owens, *Microsyst. Nanoeng.* **2017**, *3*, 17028.
[15] A. V. Nguyen, A. Y. Shourabi, M. Yaghoobi, S. Zhang, K. W. Simpson, A. Abbaspourrad, *PLoS One* **2022**, *17*, 0272294.
[16] P.-C. Tang, O. Eriksson, J. Sjögren, N. Fatsis-Kavalopoulos, J. Kreuger, D. I. Andersson, *Front Cell Infect Microbiol* **2022**, *12*, 896149.
[17] K. Wen, A. A. Gorbushina, K. Schwibbert, J. Bell, *ACS Biomater. Sci. Eng.* **2024**, *10*, 4626.
[18] J. Schwarze, R. Wanka, A. Rosenhahn, *Biointerphases* **2020**, *15*, 031014.
[19] N. Blanco-Cabra, M. J. López-Martínez, B. V. Arévalo-Jaimes, M. T. Martin-Gómez, J. Samitier, E. Torrents, *NPJ Biofilms Microbiomes* **2021**, *7*, 62.
[20] S. Zheng, D. Carugo, F. Clavica, A. Mosayyebi, S. Waters, *in Urinary Stents*, Springer, Berlin **2022**.
[21] H. Kamada, M. Nakamura, H. Ota, S. Higuchi, K. Takase, *J Cardiol* **2022**, *80*, 386.
[22] E. Tsagkari, S. Connelly, Z. Liu, A. McBride, W. T. Sloan, *NPJ Biofilms Microbiomes* **2022**, *8*, 33.
[23] G. Wei, J. Q. Yang, *NPJ Biofilms Microbiomes* **2023**, *9*, 73.
[24] H. Straub, L. Eberl, M. Zinn, R. M. Rossi, K.-M. Weber, Q. Ren, *J Nanobiotechnology* **2020**, *18*, 166.
[25] K.-W. Kim, Y. H. Choi, S. B. Lee, Y. Baba, H.-H. Kim, S.-H. Suh, *Comput Math Methods Med* **2017**, *2017*, 5172641.
[26] Q. Yu, J. Li, Y. Zhang, Y. Wang, L. Liu, M. Li, *Sci. Rep.* **2016**, *6*, 26667.
[27] T. J. Zajd, M. B. Baruch, G. Méhes, E. Stavrinidou, M. Berggren, M. M. Maharbiz, D. T. Simon, C. M. Ajo-Franklin, *Sci Rep* **2018**, *8*, 15293.
[28] S.-Y. Lien, P.-C. Lin, W.-R. Chen, C.-H. Liu, K.-W. Lee, N.-F. Wang, C.-J. Huang, *Crystals (Basel)* **2022**, *12*, 1109.
[29] S. Ray, S. Löffler, A. Richter-Dahlfors, *Adv. Sci.* **2024**, *11*, 2307322.
[30] S. Gomez-Carretero, B. Libberton, K. Svennersten, K. Persson, E. Jager, M. Berggren, M. Rhen, A. Richter-Dahlfors, *NPJ Biofilms Microbiomes* **2017**, *3*, 19.
[31] R. Sandeep, J. F. Muscolino, W. V. Macêdo, M. Piculell, M. Christensson, J. S. Poulsen, J. L. Nielsen, L. Vergeynst, *Water Res.* **2023**, *245*, 120599.
[32] E. E. Mann, D. J. Wozniak, *FEMS Microbiol. Rev.* **2012**, *36*, 893.
[33] J. V. Green, T. Kniazeva, M. Abedi, D. S. Sokhey, M. E. Taslim, S. K. Murthy, *Lab Chip* **2009**, *9*, 677.
[34] Y. D. N. Tremblay, P. Vogeleer, M. Jacques, J. Harel, *Appl. Environ. Microbiol.* **2015**, *81*, 2827.
[35] J. Kim, M. Hegde, S. H. Kim, T. K. Wood, A. Jayaraman, *Lab Chip* **2012**, *12*, 1157.
[36] I. Chopra, M. Roberts, *Microbiology and Molecular Biology Reviews* **2001**, *65*, 232.
[37] M. Moffa, I. Brook, *Elsevier* **2015**, *1*, 322.
[38] Y. Morita, J. Tomida, Y. Kawamura, *Front Microbiol* **2014**, *4*, 422.
[39] R. A. Proctor, C. von Eiff, B. C. Kahl, K. Becker, P. McNamara, M. Herrmann, G. Peters, *Nat. Rev. Microbiol.* **2006**, *4*, 295.
[40] D. Nguyen, A. Joshi-Datar, F. Lepine, E. Bauerle, O. Olakanmi, K. Beer, G. McKay, R. Siehnel, J. Schafhauser, Y. Wang, B. E. Britigan, P. K. Singh, *Science* **1979**, *334*, 982.
[41] J. Yan, B. L. Bassler, *Cell Host Microbe* **2019**, *26*, 15.
[42] H. M. Abuzeid, C. M. Julien, L. Zhu, A. M. Hashem, *Crystals (Basel)* **2023**, *13*, 1576.
[43] N. Bourguignon, V. Kamat, M. Perez, K. Mathee, B. Lerner, S. Bhansali, *Appl. Microbiol. Biotechnol.* **2022**, *106*, 2729.
[44] H. Niu, J. Gu, Y. Zhang, *Signal Transduct Target Ther* **2024**, *9*, 174.
[45] J. Wille, T. Coenye, *Biofilm* **2020**, *2*, 100027.
[46] N. Bourguignon, M. Alessandrello, R. Booth, C. B. Lobo, M. S. Juárez Tomás, L. Cumbal, M. Perez, S. Bhansali, M. Ferrero, B. Lerner, *Chemosphere* **2022**, *303*, 135001.
[47] Y. Lv, H. Liu, Z. wang, L. Hao, J. Liu, Y. Wang, G. Du, D. Liu, J. Zhan, J. Wang, *Polym. Adv. Technol.* **2008**, *19*, 1455.